Pertanika J. Sci. & Technol. 26 (3): 1489 - 1504 (2018)

SCIENCE & TECHNOLOGY

Journal homepage: http://www.pertanika.upm.edu.my/

Adaptive MOEMS Based Micro Pressure Sensor Using Photonic Crystal

Johnson, O. V.[1]* and Preeta Sharan[2]

[1]*Research and Development Centre, Bharathiar University, Coimbatore, Tamilnadu, India*
[2]*Department of E&C Engineering, Oxford College of Engineering, Bangalore, Karnataka, India*

ABSTRACT

The Micro Opto Electro Mechanical System (MOEMS) is a most promising cutting-edge technology development that uses recent trends and has huge potential for use in sensing applications. This simulation study describes the Photonic Crystal- (PhC) based micro pressure sensor, which is highly position-sensitive and free from external electromagnetic interference. Functionality of MOEMS in the photonic crystal-based micro pressure sensor is achieved through the movement of the two piston-shaped slab structures analysed in Rods in Air (RIA) and Holes in Slab (HIS) that belong to photonic crystal configurations. Displacement of the micro cavity due to applied pressure gives rise to shifts in wavelength. It is found that for each submicron displacement starting from 0 to 0.25 mm of the piston-shaped slab that is embedded, an approximate range of wavelength shift of 0.0001 for rods in air and for holes in slab configurations occurs. The simulation design shows a remarkable response in terms of intensity shift for desirable range of wavelengths 1.36 μm to 1.44 μm for RIA and 1.377 to 1.382 for HIS, thus confirming that wavelength is adaptable. The performance parameters such as Q factor and deflection range for wavelength and intensity are observed for both RIA and HIS configurations and it is found that the sensor with the HIS configuration shows better performance with Q factor of 15897 compared with the sensor with RIA configuration, which remained at a Q factor of 2482. Deformation of structure for applied pressure exhibits a linear relationship with a resonant wavelength shift. Structural variation in relation to wavelength shift exhibits a pressure sensitivity of 58.4 μm/Pa and 0.98 μm/μPa for each configuration.

Keywords: Photonic crystal, rod in air, holes in micro cavity, Perfectly Matching layer (PML), pressure, total direct strain, Finite Difference Time Domain (FDTD)

ARTICLE INFO

Article history:
Received: 20 November 2017
Accepted: 28 June 2018

E-mail addresses:
johnson.ov@christuniversity.in (Johnson, O. V.)
sharanpreeta@gmail.com (Preeta Sharan)
*Corresponding Author

ISSN: 0128-7680

INTRODUCTION

Photonic crystal (Sheikhaleh, Abedi, & Jafari, 2016) has a periodic optical structure that controls the flow of light by affecting the motion of photons much in the same way

as solid ionic lattices affect electrons. Photonic crystal is available in one-dimensional, two-dimensional and three-dimensional configurations. Photonic crystal used as a sensor (Kovacs, Ivanov, & Mescheder, 2015) is used widely in most applications because of their advantageous physical characteristics such as being highly sensitive and having transmittance and reflectance. By using 1D, 2D, or 3D photonic crystal structure, it is possible to control the flow of light; this is not possible using conventional optical materials (Trigona, Ando, & Baglio, 2016). A combination of the optical and mechanical system to actuate the electrical structure developed is known as the Micro Opto Electro Mechanical System (MOEMS). A MOEMS micro sensor uses an input signal sensed by a micro sensor element that is transduced by a transduction unit to produce an output signal. Using the optical system along with MEMS technology (Yang, Tian, Wu, Yang, & Ji, 2013) allows for a lot of benefits such as low weight, micro size, elimination of cross talk or electromagnetic interference and immunity to variation in temperature and moisture content. MOEMS uses many advanced fabrication technologies in micromachining (Biallo, Sario, Orazio, & Marrocco, 2007), encapsulations and die bonding, among others. A more extensively developed technology for the MOEMS pressure sensor is micromachining, which mostly uses capacitive piezo resistive or resonant frequency technology. These techniques mould pressure into displacement or strain it through a membrane (Tung, Dao, & Sugiyama, 2010).

In one work, the force and strain sensing capability of the noval PhCWG- (Yablonovith, 1994) based bridge structure was studied. A pair of air holes in a silicon linear waveguide acted as a reflector. A free standing bridge beam structure was proposed comprising a photonic crystal waveguide for strain and force sensing, as the beam structure is a common mechanical structure used in MEMS-based physical sensors (Bahaddur, Srikanth, & Sharan, 2016). It was concluded that a change in defect length coupled with an elongation and or deformation in x direction would be the most sensitive parameter to resonant wavelength shift (Motamedi, 2010). A novel nano-scale optical torsion-free photonic crystal pressure sensor was analysed. It consisted of a PhC waveguide and side-coupled piston-type micro cavity. During the analysis, optical properties of resonant mode on the applied strain were systematically studied (Imada Noda, Chutinan, Mochizuki, & Tanaka, 2002). A linear relationship between applied strain and shift in wavelength with pressure sensitivity of 0.50 nm/nN was seen. Work was accomplished relevant to a tunable PhC sensor that was highly sensitive to position where the polysilicon micro cavity with silicon pillars were incorporated. MEMS flexures (Levy, Steinberg, Boag, Krylov, & Farb, 2007), using two-dimensional photonic crystal cavities where photonic crystal mounted on flexures, were used; the deformation was transferred to the photonic crystal. Defects were introduced in the photonic crystal and it was analysed with a mechanical flexure using the silicon as a material with consistent characterisation.

The photonic crystal sensor (Choudhury, 2009) has been intensively studied for change of refractive index as variation in pressure can shift the resonant wavelength, in turn inducing change in the refractive index of structure. Investigation of the optical sensor related to MEMS technology (Radhakrishnan & Chen, 2008) has proven to be useful in a wide area of applications like microfluidics and blood pressure measurement, among others. In this paper, the function of a novel micro-scale MOEMS-based micro pressure sensor (Zamora, 2011) using photonic crystal technology (Boutami et al., 2007) was demonstrated. Then design consisted of two

inverted piston-type slab structures (Subramanian, Upadhyaya, & Sharan, 2017) coupled with photonic crystal configurations. The performance parameters such as Q factor, sensitivity and deflection range for wavelength and intensity for applied pressure were scrutinised for two different configurations of the photonic crystal. Characterisation and simulation of the MOEMS device (Zouache, Hocini, Harhouz, & Mokhtari, 2016) used photonic crystal technology to observe change in the peak resonance mode of transmission spectrum due to deformation of the micro cavity in the PhC after applying pressure. Structural variations due to the applied pressure (Shakhnov & Zinchenko, 2014) for the piston-type slab structure were studied and strain due to mechanical deformation evaluated by finite element analysis. The proposed piston-type micro cavity coupled with photonic crystal configuration in an array of slabs was observed.

DESIGN APPROACH AND WORKING PRINCIPLE

The architecture of the proposed micro pressure sensor using photonic crystal is shown in Figure 1. The design approach involved the design of photonic crystal for rods in air configuration and holes in slab configuration and Gaussian pulse source and was kept at the centre of two piston-type micro cavity structures. Finite Difference Time Domain (FDTD) solves mathematical equations representing electric and magnetic field effects. This interaction of current and magnetic fields with one another and with matter and source uses the Maxwell equation and was analysed in MIT electromagnetic wave propagation (MEEP). Using the FDTD code form behind the tool MEEP provided the output of transmission spectrum and computed fluxes for the specified equations. The PML Boundary Layer or nonphysical boundary condition controlled the confinement of the light propagation within the waveguide. Two piston-shaped micro cavities made of silicon were embedded in the photonic crystal rods in air and holes in micro cavity configurations.

Table 1
Parameters of PhC configurations

Type lattice structure	Square Lattice
Lattice constant ‘a’	1 μm
Radius of rods ‘r’	0.17 μm (For rods in air configuration)
Radius of holes	0.17 μm (For holes in micro cavity configuration)
Refractive index of air	1.000293
Dielectric constant of silicon rods	11.74
Wavelength of light ‘λ’	1550 nm
Total frequency to which flux is calculated during MEEP simulation	500
Light source used	Gaussian pulse of frequency 0.4 and width of pulse 0.3

When pressure was applied on the two ends of the piston-shaped micro cavity, both micro cavities were considered to be moving towards each other. Movement of piston type structure was made for micron range. In the present work, the micro cavity was displaced by 0 to 0.25 μm value in an increment of 0.05 μm. Pulses of Gaussian light source passed through the slab,

as shown in Figures 3(a), 3(b), 3(f) and Figures 5(a) and 5(c). The propagation of light can be seen throughout the micro cavity, due to the presence of the PML Layer, which absorbed the most reflected light waves and confined the light on the slab that had less dispersion. As the micro cavities were displaced, electromagnetic waves passing through the piston-type slab structure were transmuted, shifting the wavelength transmuting the transmission spectrum. The corresponding Maxwell equations governing the photonic crystal light propagation were:

$$\nabla . B = 0 \quad \nabla \times E + \frac{\partial B}{\partial t} = 0 \tag{1}$$

where, B = magnetic flux density; J is current density; E = electric field; H = magnetic field

$$\nabla . B = 0 \quad \rho . \nabla \times H - \frac{\partial D}{\partial t} = J \tag{2}$$

where, D = displacement field; ρ = density

$$S_{\lambda\text{-}n} = \frac{\lambda 2 - \lambda 1}{n2 - n1} \tag{3}$$

where, $S_{\lambda\text{-}n}$ = sensitivity ; λ2-λ1 = difference in wavelength ; n2-n1 = refractive index difference.

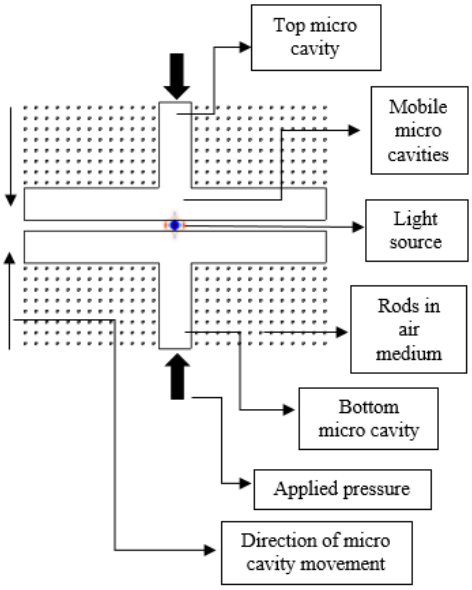

Figure 1. Photonic crystal configuration

RESULTS AND DISCUSSION

Referring to Figure 2 for the rods in air configuration, the slab was moved in the direction shown in Figure 1. Pressure was applied as shown in Figure 1 and Figure 2, and the slab was displaced to an increment of 0.05 μm from the initial position. Light was propagated from the

source centre to throughout the micro cavity, giving remarkable confinement for a particular frequency as both the micro cavity moved as shown in Figures 3(a) and 3(b). Figure 3(c) shows index distribution for the rods in air configuration. The monitors shown in Figure 2 retrieved data pertaining to wavelength and intensity variation as the slab moved from 0.05 µm to 0.25 µm. The effective index of the rods in air configuration for the proposed structure is shown Figure 3(e). Figure 3(d) depicts the 3D visualisation of the RIA configuration. The effective index of 0.991645 was identified for the RIA configuration. The index profile distribution showed the refractive index of material used during the analysis.

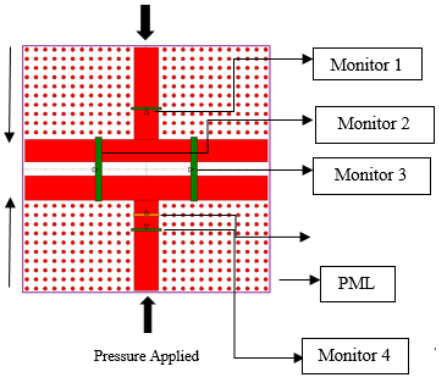

Figure 2. Photonic crystal RIA configuration with monitors

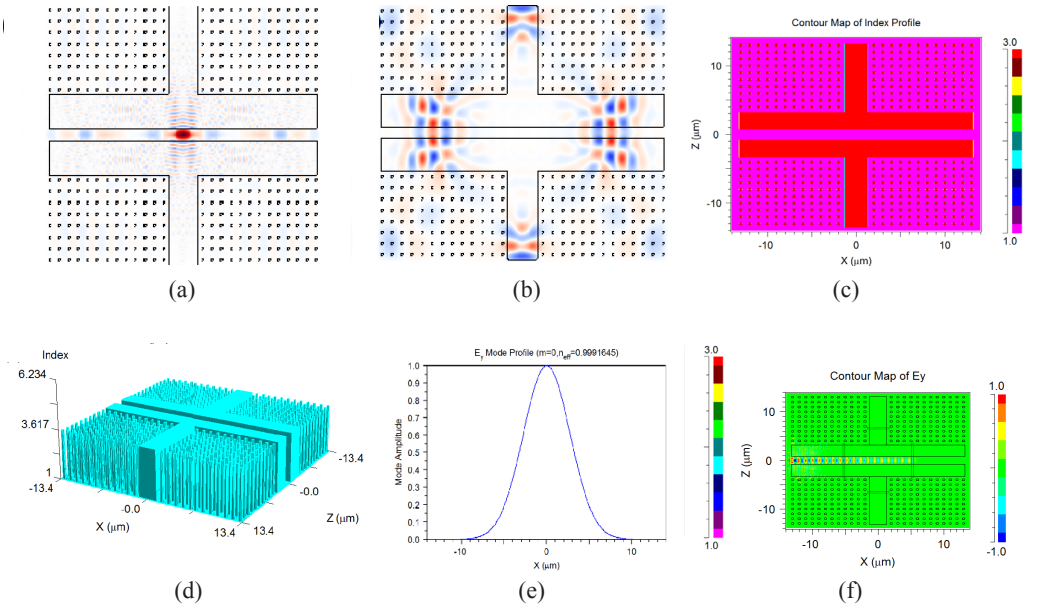

Figure 3. (a) Sample light propagation for 0.1µm displacement for RIA configuration; (b) Sample light propagation for 0.15 µm displacement of piston-shaped slab in RIA configuration; (c) Index profile distribution for RIA configuration; (d) 3D model visualisation for RIA configuration; (e) n_{eff} calculation for RIA configuration; (f) Light propagation between gaps of two piston-shaped slab

The MOEMS piston structure for holes in micro cavity configuration is shown in Figure 4. Light can be seen propagating through the proposed sensor design through the holes in the slab configuration with less dispersion, showing better confinement throughout the mobile slab. Varying flux values were obtained for each submicron displacement of the slab. Index distribution of holes in the slab configuration is indicated in Figure 5(f). n_{eff} for holes in micro cavity configuration is shown in Figure 5(e). The effective index found during the analysis was 1.888345. According to the parameters specified in Table 1, simulation was carried out allowing Gaussian pulse on the piston-shaped slab that was embedded as shown in Figures 5(a) and 5(b). The rods in air and holes in slab configurations with embedded structures used the photolithography technique to build in practical. Initially, two piston-type slabs with no displacement were used, that is no pressure was applied on the slabs. At the second level, both the inverted slabs were moved towards each other for a displacement of 0.05 µm and this was incremented at the step size of 0.05 µm. The propagation of light throughout the slab is shown in Figure 5(c).

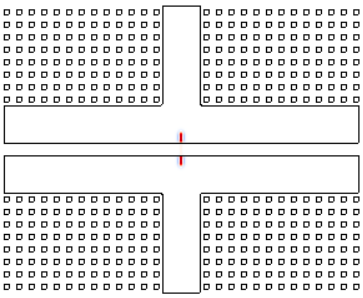

Figure 4. Proposed MOEMS-based photonic crystal micro pressure sensor in holes in micro cavity configuration

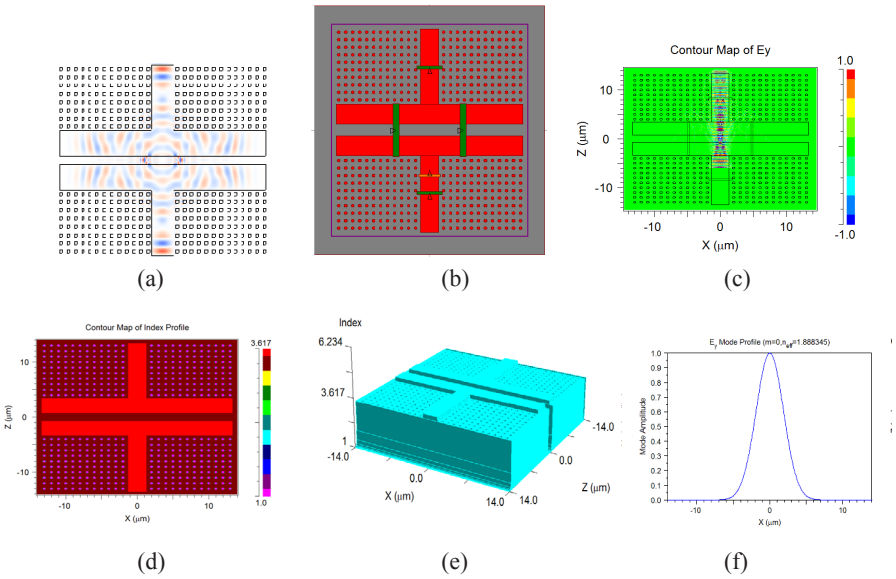

(a) (b) (c)

(d) (e) (f)

Figure 5. (a) Light propagation for 0.1µm displacement HIS configuration; (b) Photonic crystal HIS configuration with monitors; (c) Light propagation in HIS configuration; (d) Index profile distribution; (e) 3D model visualisation of HIS configuration; (f) n_{eff} calculation for HIS configuration

Figure 6(a) to Figure 6(h) show the shift in wavelength for each two displacement range 0 and 0.05 µm, 0.1 µm and 0.15 µm and 0.2 µm and 0.25 µm for rods in air and holes in micro cavity configuration. The results of the displacements and wavelength shift are shown in Table 2 and Table 3 below. The maximum Q factor approximation of 15892 was observed for the HIS configuration as indicated in Figures 7(a) and 7(b). The Q factor was analysed for changing the aspect ratio of configuration for the radius of the holes and rods, as depicted in Figure 7(b). Absorbing boundaries of structure due to pulse excitation adopted the period of time taken for light to travel from the piston-type slab structure to the surroundings and vice versa. The Finite Difference Time Domain (FDTD) method evaluated during the simulation of light travel in HIS and RIA configuration was used to analyse the decay rates to quantify the Q factor.

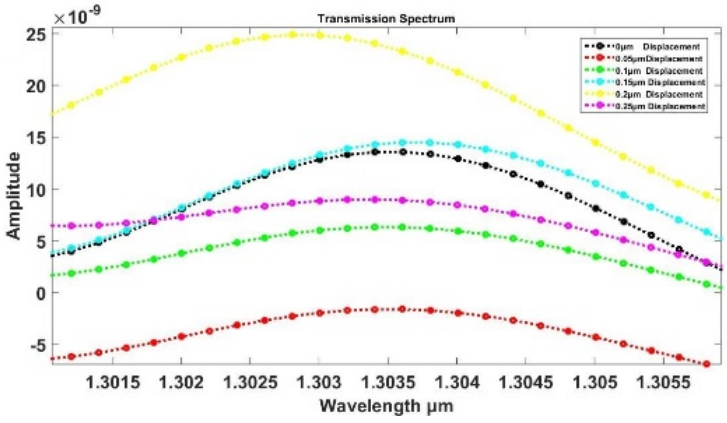

(a)

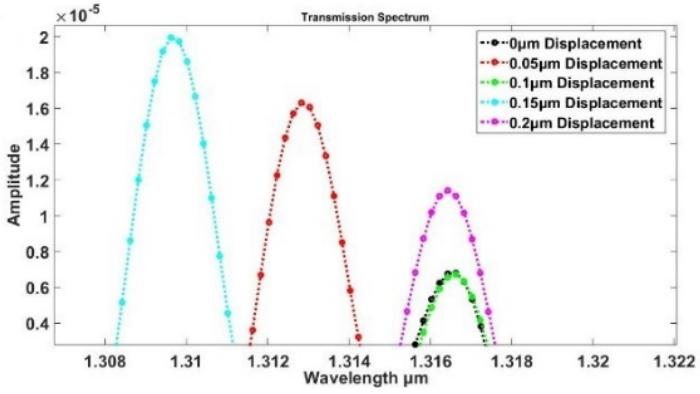

(b)

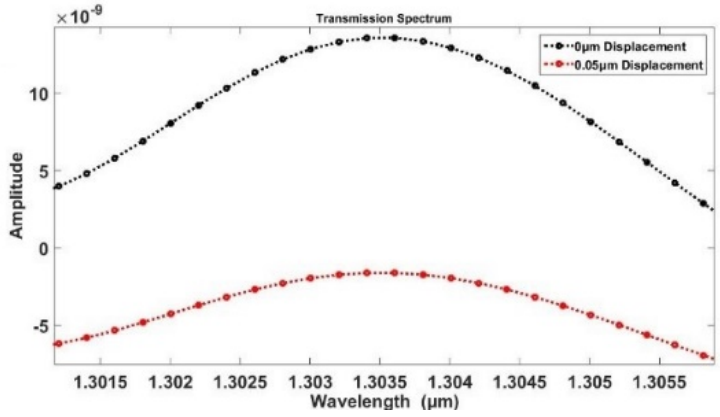
×10^-9
Transmission Spectrum
0μm Displacement
0.05μm Displacement
Amplitude
10
5
0
-5
1.3015
1.302
1.3025
1.303
1.3035
1.304
1.3045
1.305
1.3055
Wavelength (μm)

(c)

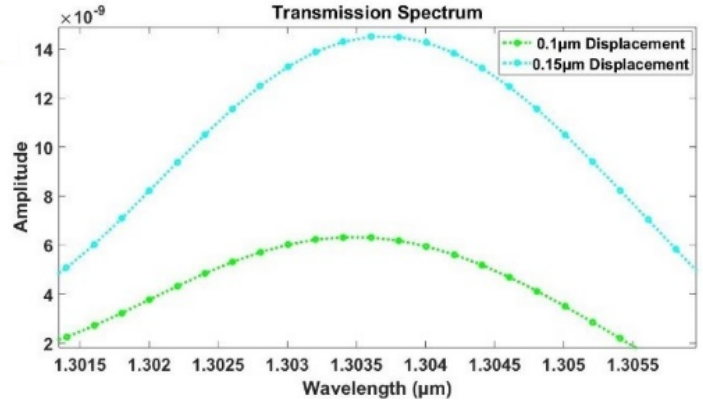
×10^-9
Transmission Spectrum
0.1μm Displacement
0.15μm Displacement
Amplitude
14
12
10
8
6
4
2
1.3015
1.302
1.3025
1.303
1.3035
1.304
1.3045
1.305
1.3055
Wavelength (μm)

(d)

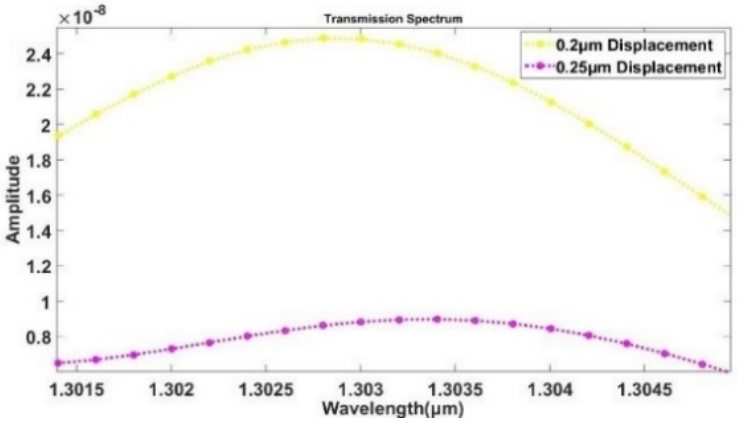
×10^-8
Transmission Spectrum
0.2μm Displacement
0.25μm Displacement
Amplitude
2.4
2.2
2
1.8
1.6
1.4
1.2
1
0.8
1.3015
1.302
1.3025
1.303
1.3035
1.304
1.3045
Wavelength(μm)

(e)

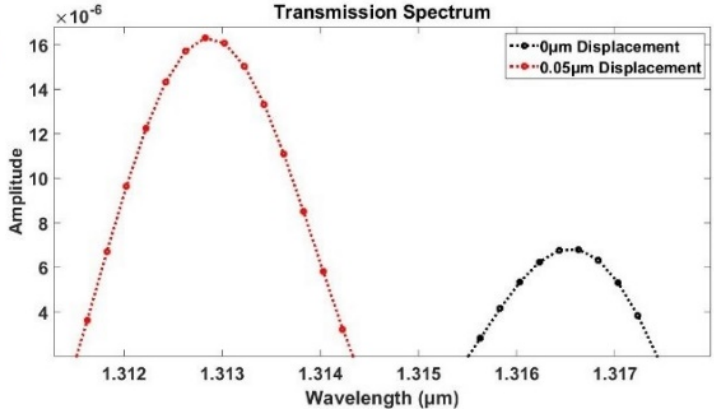

(f)

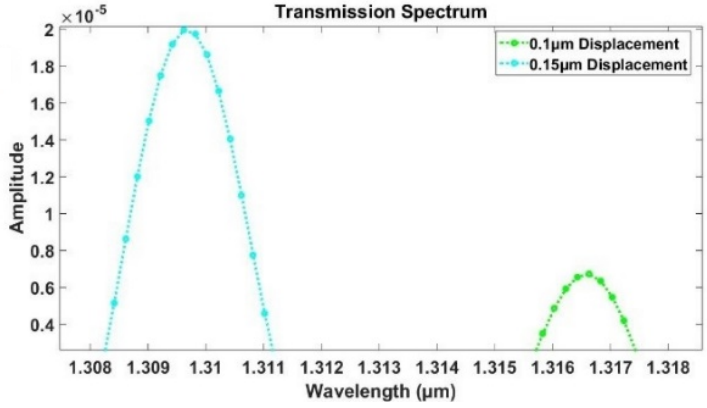

(g)

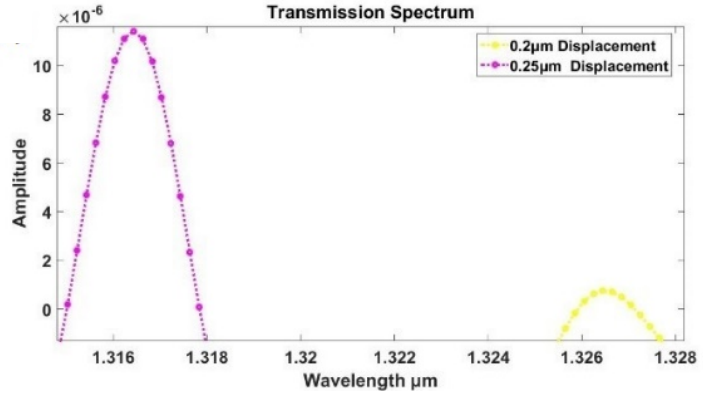

(h)

Figure 6. (a) Combined spectral behaviour of wavelength shift for RIA configuration; (b) Combined spectral behaviour of wavelength shift for HIS configuration; (c) Distinct shift in wavelength for the 0 and 0.05 μm displacement RIA configuration; (d) Distinct shift in wavelength for the 0.1 μm and 0.15 μm displacement RIA configuration; (e) 0.2 μm and 0.25 μm displacement in the RIA configuration; (f) Distinct shift in wavelength for the 0 and 0.05 μm displacement HIS configuration; (g) Distinct shift in wavelength for the 0.1 μm and 0.15 μm displacement HIS configuration; (h) Distinct shift in wavelength for the 0.2 μm and 0.25 μm displacement HIS configuration

Table 2
Result for holes in slab configuration

Displacement	Wavelength	Wavelength shift
0	1.3033	0
0.05	1.3034	0.0001
0.1	1.3036	0.0002
0.15	1.3038	0.0002
0.2	1.3037	0.0007
0.25	1.3034	0.0003

Table 3
Result for rods in air configuration

Displacement	Wavelength	Wavelength shift
0	1.3165	0
0.05	1.3129	0.0036
0.1	1.3166	0.0037
0.15	1.3167	0.0001
0.2	1.3260	0.0093
0.25	1.3164	0.0096

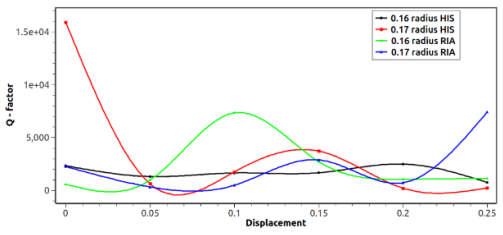

(a)

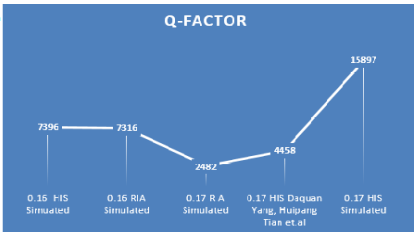

(b)

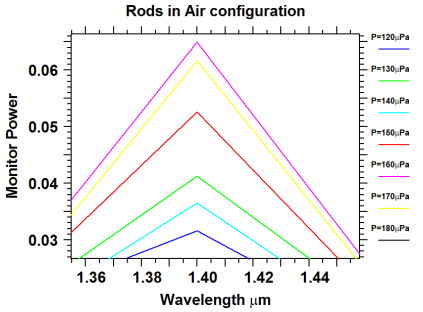

(c)

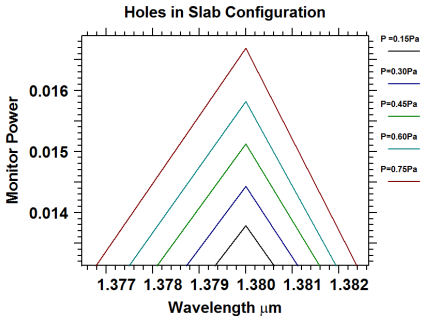

(d)

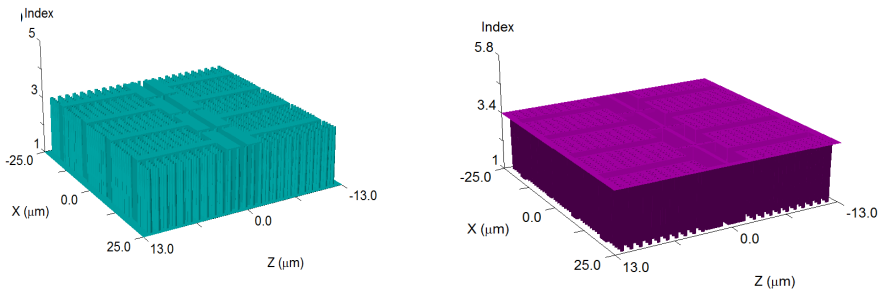

(e) (f)

Figure 7. (a) Quality factor obtained for 0.16 RIA, 0.16 HIS, 0.17 RIA and 0.17 HIS for displacement of 0 to 0.25 μm; (b) Maximum quality factor achieved by changing the aspect ratio for HIS and RIA configurations; (c) and (d) Various applied pressure and wavelength shift for RIA and HIS configurations; (e) and (f) Array of piston-type structure slabs for bulk pressure with higher accuracy

Figure 7(c) and Figure 7(d) show wavelength peak in relation to power and applied pressure. There was a shift in amplitude for each increase in pressure from 120 micro Pascal to 180 micro Pascal in the case of the rods in air configuration. Pressure varied from 0.15 Pascal to 0.75 Pascal, while power and wavelength peak were monitored by optimising the output in the holes in slab configuration. A distinct shift was observed in intensity with respect to the applied pressure in the holes in the micro cavity configuration compared with the rods in air configuration.

To study the structural response of the sensor due to variation in mechanical parameters, the proposed micro structure was modelled in Abaqus CAE as shown in Figure 8. Due to applied pressure on both ends of the piston type of slab, structural variation was exhibited, resulting in mechanical distortion and the linear perturbation method was adopted to analyse the designed structure. A mapped quad mesh was generated using the model as shown in Figure 9(a), and suitable boundary conditions and constraints were assigned as per the movement of the sensor structure. Force was applied at both ends of the piston structure, such that back and forth movement of the structure was noticed. For each increase in the force, increase in the overall displacement of structure was identified in Figure 9(c).

$$\varepsilon = \frac{\sigma}{E} \text{ or } \mu = \frac{|\in lateral|}{|\in axial|} \tag{4}$$

$$\epsilon_x = \sigma_x / E \tag{5}$$

where, ε = strain, σ = stress, E = Young's modulus, ϵ_x= strain in x direction, σ_x= stress in x direction

$$\text{Strain} = \Delta L / L \tag{6}$$

where, ΔL = change in dimension, L= initial dimension

Young's modulus of silicon (E) = 150Gpa, Poisson's ratio (μ) = 0.14, Density of silicon (ρ) = 2328 kg/m^{-3}, Stress acting on the structure σ.

By correlating the mechanical parameters of the HIS configuration, we analysed the VonMises stress and total direct strain distribution of the micro structure for each increase in force. Figure 9(c) and Figure 9(d) shows stress and strain distribution in the proposed micro structure. Structural variation due to applied pressure with respect to wavelength shift decided the pressure sensitivity of the piston-type structure in both the configurations of the photonic

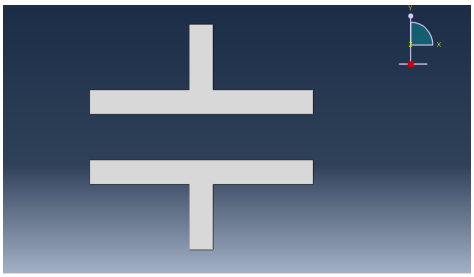

Figure 8. CAD model of proposed micro structure

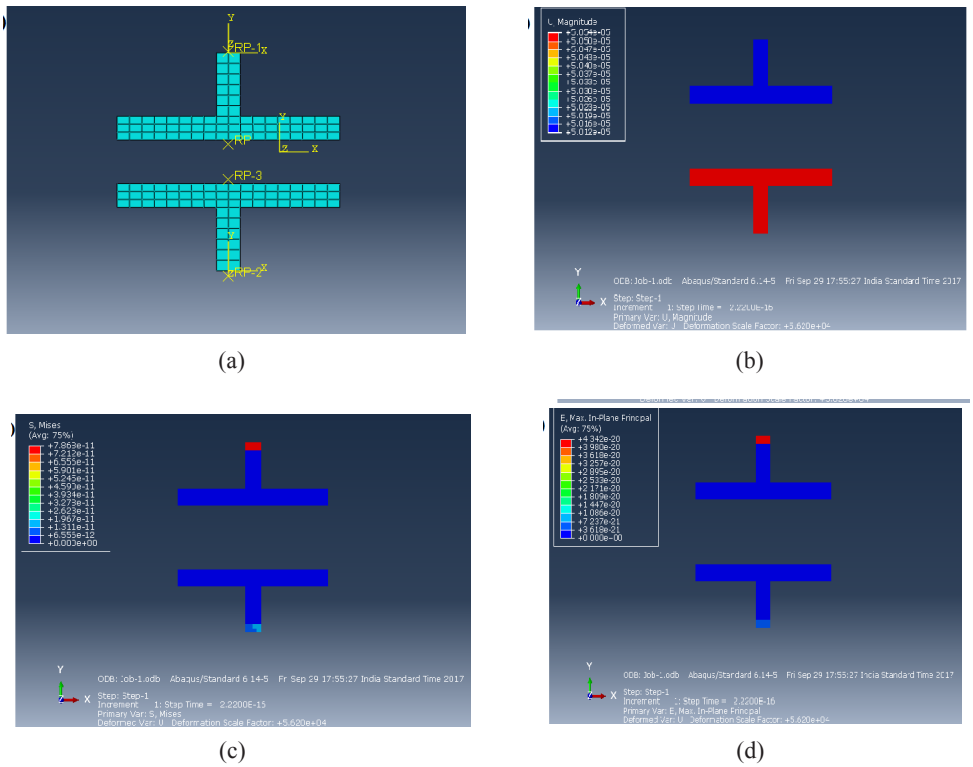

Figure 9. (a) FEA discretisation of the proposed structure; (b) Displacement behaviour of the proposed structure for applied pressure; (c) Sample stress behaviour of proposed structure; (d) Strain simulation for piston-type structure

crystal structure. Due to the stability feature of the HIS and RIA configuration for micron level movements of the piston-type slab, pressure sensitivity of 58.4 μm/Pa was recorded for the rods in air configuration, while for the holes in slab configuration, it was 0.98 μm/Pa.

The CAD model was developed by considering the same design parameters as those used in the photonic-based MOEMS structure shown in Figure 8. The designed CAD model is capable of showing the same behaviour as that in photonics. The basic fact behind the FEA analysis was to obtain the mechanical displacement and strain caused due to applying micron-level pressure. Linear relationship between wavelength shift and strain was observed during the analysis as shown in Figure 10(c). Further simulation with Abaqus FEA was performed to observe the stress behaviour for the piston-type structure. This analysis for mechanical behaviour was based purely on Hooke's law. Graphical representation shown in Figure 10(a) shows a linear relationship between stress and strain for the varying pressure units. Figure 10(b) captures the behaviour of strain against wavelength. The graph shows that there was a gradual increase of wavelength shift for strain ranging from 0.5e-19 to 1.4e-^{19}. An abrupt increase in wavelength shift was observed after the direct strain value of 1.4e-^{19}.

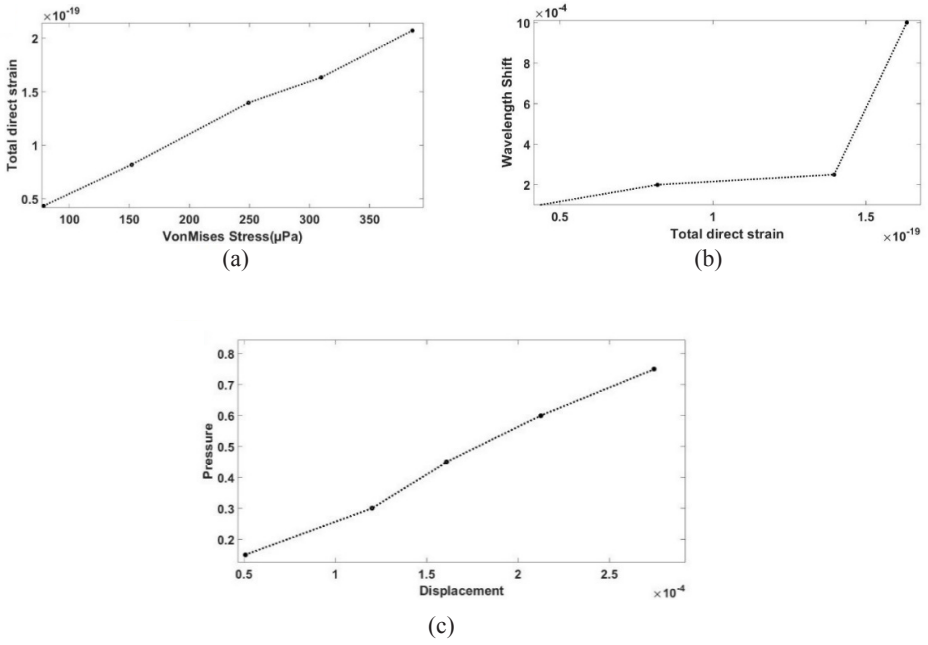

Figure 10. (a) Stress vs strain; (b) Linear relationship between wavelength shift and strain; (c) Applied pressure and displacement behaviour

CONCLUSION

This paper documents the use of an adaptive MOEMS micro pressure sensor using photonic crystal technology. The proposed sensor depends on the movement of two piston-type slabs embedded in RIA and HIS configurations. Simulation wavelength and intensity modulation were achieved for change in the mechanical parameters such as displacement and pressure. Using FDTD, the behaviour of photonic crystal-based pressure sensing technology was investigated. The simulation results showed that shifts in wavelength and intensity for varied pressure units in relation to wavelength. A maximum quality factor of 15897 was obtained for the holes in slab configuration compared with a quality factor of 2482 obtained for the rods in air configuration for a radius of 0.17 μm, while a Q factor of 7396 was obtained for the holes in slab configuration and 7316 for the rods in air configuration for a radius of 0.16 μm. A distinct intensity shift for a desirable range of wavelength from 1.3 μm to 1.38 μm was obtained in the holes in micro cavity configuration, and this was found to be remarkable compared with the shift obtained for the rods in air configuration. Linear behaviour of strain with respect to resonant wavelength shift was observed during analysis of the mechanical parameters. A sensitivity of 54.8 μm/Pa and 0.98 μm/Pa was achieved for the rods in air and holes in slab configurations, respectively.

The proposed sensor provides various benefits such as reliability and protection from electromagnetic interference. The results of this study showed that the design parameters and specifications greatly influenced sensor performance, including sensitivity, selectivity and sensing range. It was also shown that the sensing range could be adjusted and also that sensor sensitivity can be enhanced using the optimised design parameters. This type of sensor has tremendous application potential in biomedical instrumentation, especially for determining the blood pressure of neonatal babies.

ACKNOWLEDGEMENT

Authors are grateful to all the researchers for their assistance in carrying out work as well as for their meaningful suggestions during the project and for helping to moderate this paper, a task that improved the manuscript significantly.

REFERENCES

Bahaddur, I., Srikanth, P. C., & Sharan, P. (2016). *Photonic crystal nano cavity pressure sensor*. India: OSA Publishing. https://doi.org/10.1364/PHOTONICS.2016.Tu4A.69

Biallo, D., Sario, M., Orazio, D., & Marrocco, V. (2007, May). High sensitivity photonic crystal pressure sensor. *Journal of the European Optical Society Rapid Publications, 2*(2007), 1-5. doi: 10.2971/jeos.2007.07017

Boutami, S., Bakir, B. B., Leclercq, J. L., Letartre, X., Seassal, C., Rojo-Romeo, P., ... & Viktorovitch, P. (2007). Photonic crystal-based MOEMS devices. *IEEE Journal of Selected Topics in Quantum Electronics, 13*(2), 244–252.

Choudhury, P. R. (2009). *MEMS and MOEMS Technology and Applications.* India: PHI Publication Edition.

Imada, M., Noda, S., Chutinan, A., Mochizuki, M., & Tanaka, T. (2002, May). Channel drop filter using single defect in a 2D photonic crystal micro cavity waveguide. *Journal of Light Wave Technology, 20*(5), 873–878. https://zapdf.com/channel-drop-filter-using-a-single-defect-in-a-2-d-photonic.html

Kovacs, A., Ivanov, A., & Mescheder. (2015). Tunable narrow band photonic crystal for MOEMS based scanning systems. *Euro Sensor, 120*, 811–815. https://doi.org/10.1016/j.proeng.2015.08.669

Levy, O., Steinberg, B. Z., Boag, A., Krylov, I., & Farb, G. (2007). Mechanical tuning of two dimensional photonic crystal cavity by micro electro mechanical flexures. *Sensors and Actuators A: Physical, 139*(1-2), 47–52. https://doi.org/10.1016/j.sna.2006.11.018.

Motamedi, M. E. (2010). *MOEMS.* India: New Age International (P) Ltd.

Radhakrishnan, R., & Chen, C. C. (2008). Design and modelling of nano mechanical sensor using silicon photonic crystal. *Journal of Light Wave Technology, 26*(27), 839–846. doi: 10.1109/JLT.2007.915273

Shakhnov, V. A., Zinchenko, L. A., & Kosolapov, I. A. (2014, October). Simulation of distributed MOEMS for smart environments. In *10th International Conference on Advanced Semiconductor Devices & Microsystems (ASDAM), 2014* (pp. 1–4). IEEE.

Sheikhaleh, A., Abedi, K., & Jafari, K. (2016). A proposal for an optical MEMS accelerometer relied on wavelength modulation with one dimension photonic crystal. *Journal of Light wave Technology, 34*(22), 5244–5249. doi: 10.1109/JLT.2016.2597539

Subramanian, S., Upadhyaya, A. M., & Sharan, P. (2017, August). MOEMS-based accelerometer sensor for supplementary restrain system in automobile passenger safety. *Indian Journal of Science and Technology, 10*(29), 1-6. doi: 10.17485/ijst/2017/v10i29/117327

Trigona, C., Ando, B., & Baglio, S. (2016). Fabrication and characterization of an MOEMS Gyroscope based on photonic band gap materials. *IEEE Transactions on Instrumentation and Measurement, 65*(12), 2840–2852. doi: 10.1109/TIM.2016.2608078

Tung, B. T., Dao, D. V., & Sugiyama, S. (2010, August). Investigation of strain sensitivity of photonic crystal nanocavity for mechanical sensing. In *International Conference on Optical MEMS and Nanophotonics (OPT MEMS), 2010* (pp. 183–184). IEEE.

Yablonovith, E. (1994). Photonic crystals. *Journal of Modern Optics, 41*(2), 173–194. https://doi.org/10.1080/09500349414550261

Yang, D., Tian, H., Wu, N., Yang, Y., & Ji, Y. (2013). Nanoscale torsion-free photonic crystal pressure sensor with ultra-high sensitivity based on side-coupled piston-type microcavity. *Sensors and Actuators A: Physical, 199*, 30–36. https://doi.org/10.1016/j.sna.2013.04.022

Zamora, R. (2011). Optical characterization of photonic crystals as polarizing structure for tunable MEMS devices. In M. Kusserow & H. Hilmer (Eds.). *16th International Conference on optical MEMS and Nanophotonics* (pp. 83-84). IEEE. doi: 10.1109/OMEMS.2011.6031069

Zouache, T., Hocini, A., Harhouz, A., & Mokhtari, R. (2017). Design of pressure sensor based on two-dimensional photonic crystal. *Acta Physica Polonica A, 131*(1), 68–70.